Cell

Crystal Structures of a Ligand-free MthK Gating Ring: Insights into the Ligand Gating Mechanism of K^+ Channels

Sheng Ye,[1] Yang Li,[1] Liping Chen,[1] and Youxing Jiang[1,*]
[1] Department of Physiology, University of Texas Southwestern Medical Center, Dallas, TX 75390, USA
*Contact: youxing.jiang@utsouthwestern.edu
DOI 10.1016/j.cell.2006.08.029

SUMMARY

MthK is a prokaryotic Ca^{2+}-gated K^+ channel that, like other ligand-gated channels, converts the chemical energy of ligand binding to the mechanical force of channel opening. The channel's eight ligand-binding domains, the RCK domains, form an octameric gating ring in which Ca^{2+} binding induces conformational changes that open the channel. Here we present the crystal structures of the MthK gating ring in closed and partially open states at 2.8 Å, both obtained from the same crystal grown in the absence of Ca^{2+}. Furthermore, our biochemical and electrophysiological analyses demonstrate that MthK is regulated by both Ca^{2+} and pH. Ca^{2+} regulates the channel by changing the equilibrium of the gating ring between closed and open states, while pH regulates channel gating by affecting gating-ring stability. Our findings, along with the previously determined open MthK structure, allow us to elucidate the ligand gating mechanism of RCK-regulated K^+ channels.

INTRODUCTION

Ion selectivity and channel gating are the two basic properties that define an ion-channel function. All K^+ channels contain a conserved amino acid sequence and structure within their pore to accomplish ion selection, as exemplified by the structure of the KcsA K^+ channel from *Streptomyces lividans* (Doyle et al., 1998; Zhou et al., 2001). In K^+ channels, four pore-lining inner helices form a bundle crossing at the intracellular surface of the membrane. This bundle is too small (~4 Å) to permit hydrated ions to pass and must come apart in an open channel, making it the likely location of a K^+-channel "gate" (del Camino et al., 2000; del Camino and Yellen, 2001; Liu et al., 1997, 2001; Perozo et al., 1999). In ligand-gated channels, conformational changes induced by ligand binding lead to the opening of the gate. Unlike the conserved ion-conduction pore, the protein modules underlying ligand gating vary among K^+ channels, owing to a wide range of ligand molecules.

The majority of prokaryotic K^+ channels contain a conserved C-terminal ligand-binding domain termed the RCK domain for its role in *r*egulating the *c*onductance of K^+ (Jiang et al., 2001; Kuo et al., 2005). The ligands for RCK domains are diverse: Some RCK domains have a conserved sequence motif for NAD^+ binding (Bellamacina, 1996), but others do not. RCK domains are also ubiquitously distributed in bacterial K^+ uptake (Trk or Ktr systems) (Nakamura et al., 1998; Schlosser et al., 1993) and efflux machinery (Kef systems) (Bakker et al., 1987; Munro et al., 1991). In K^+-uptake systems, RCK exists as an individual cytoplasmic protein called TrkA or KtrA and assembles with the pore-forming membrane-spanning unit (TrkG/H or KtrB). The N-terminal two-thirds of an RCK domain (~150 residues) has a Rossmann-folded structure (Rossmann et al., 1974) and is referred to as the KTN domain in K^+ transporters for its role in regulating K^+ *t*ransport and *n*ucleotide binding (PF02254 in the Pfam protein domain/family database) (Bateman et al., 2000). Structure-based sequence alignment and mutagenesis studies have shown that RCK domains also exist in eukaryotic large-conductance Ca^{2+}-gated K^+ channels (BK or maxiK channels) as two tandem repeats at the intracellular C-terminal side (Jiang et al., 2001, 2002a; Pico, 2003). The wide distribution of RCK domains in K^+ channels and transporters highlights their importance in regulating the flow of K^+ across the cell membrane.

RCK domains are α/β proteins that associate as homodimers with a bilobed architecture (Dong et al., 2005; Jiang et al., 2001; Roosild et al., 2002). However, the dimer form of RCK domains observed in most structures does not represent their native functional assembly and therefore provides limited information about channel gating. The recent X-ray structure of the MthK channel in a ligand-bound open state reveals the functional assembly of the RCK domains (Jiang et al., 2002a). MthK is a Ca^{2+}-gated K^+ channel from *Methanobacterium thermoautotrophicum* that, like most K^+ channels, functions as a tetramer. Each subunit has two membrane-spanning segments that form the ion-conduction pore and a Ca^{2+}-binding RCK domain at the C terminus. The structure

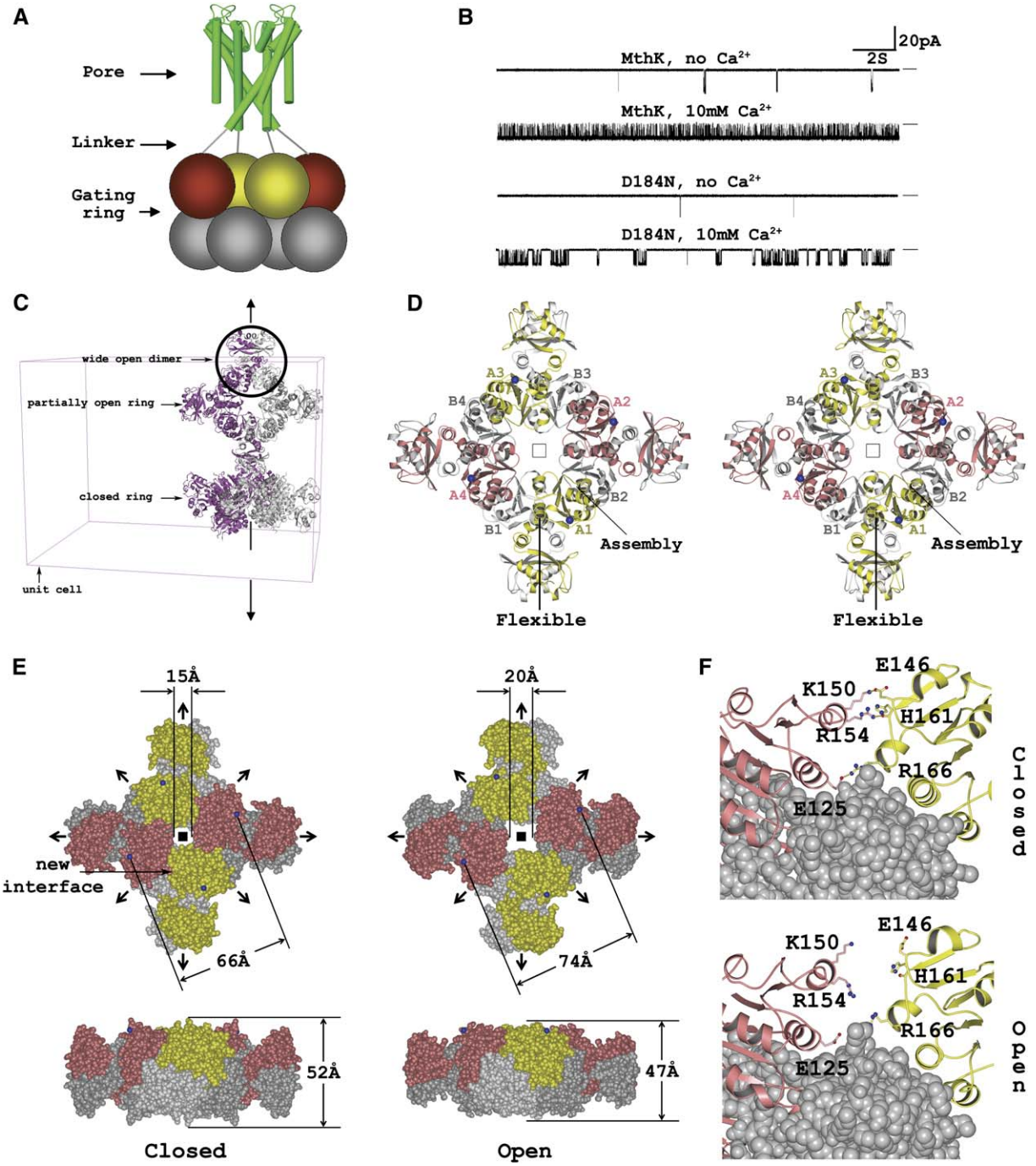

Figure 1. Overall Structure of the Closed MthK Gating Ring

(A) In MthK, eight RCK domains (spheres) form a gating ring at the intracellular side of the pore (green cylinders; modeled based on the KcsA structure, PDB ID code 1K4C). The top four RCK domains (yellow and brown) are connected to the pore through four peptide linkers (gray lines).

(B) Single-channel traces of wild-type MthK and D184N mutant in the absence and presence of 10 mM $CaCl_2$. Currents were recorded in synthetic lipid bilayers at −100 mV with an intracellular pH of 8.0 and 150 mM symmetrical KCl. Lines to the right mark the zero current level. The slight decrease of channel conductance at 10 mM Ca^{2+} is due to rapid blocking by Ca^{2+}.

(C) The eight RCK subunits in the asymmetric unit (magenta) are involved in the assembly of two gating rings with their crystallographic 2-fold (arrow) related counterparts (gray). The gating ring on top is in a partially open state; the one on the bottom is in a closed state. The wide-open flexible dimer in the partially open ring is circled.

reveals that a functional MthK channel requires eight RCK domains to form an octameric gating ring on the intracellular side of the pore. Four RCK domains are linked to the pore-forming peptide chains, while four additional copies are expressed from the *MthK* gene utilizing an internal start site (Met107) and are coassembled in the cytosol (Figure 1A). Ca^{2+} binding induces gating-ring conformational changes, which in turn lead to opening of the pore. The pore opening is achieved by the bending of the pore-lining inner helices at a conserved glycine residue, called the gating hinge, just below the pore's selectivity filter (Jiang et al., 2002b). The bent inner helices splay open, creating a wide (~12 Å) entryway at the intracellular side of the pore. The existence of the glycine gating hinge in the ion-conduction pore has also been indicated in several other channels, such as the *Shaker* K^+ channel, the G protein-regulated inwardly rectifying K^+ (GIRK) channel, and the voltage-gated Na^+ channel (Ding et al., 2005; Jin et al., 2002; Magidovich and Yifrach, 2004; Zhao et al., 2004).

The MthK structure only provides a snapshot of the channel in the open state. Addressing the fundamental question of how ligand binding induces gating-ring conformational changes requires structural information about the gating ring in its ligand-free, closed conformation. Here we present the crystal structures of the MthK gating ring in an unliganded closed state and a partially open state. Both structures were obtained from the same crystal grown in the absence of Ca^{2+}. The closed gating ring along with the open MthK structure allows us to visualize both the open and closed conformations of the functional assembly of a K^+-channel ligand-binding domain. These structures also reveal the physical basis of the ligand gating mechanism in MthK: Ca^{2+} binding at each RCK subunit leads to an expansion of the gating ring, which in turn can exert a lateral force on the channel pore and open the channel. The partially open gating ring may represent an intermediate conformation in the gating-ring transition between open and closed states and provides an allosteric view of this transition process. Furthermore, we also demonstrate that the gating of MthK is both Ca^{2+} and pH regulated. Ca^{2+} activates the channel by stabilizing the gating ring in an open conformation, whereas pH regulates the channel by altering gating-ring stability. The gating ring only assembles at near physiological or higher pH, allowing Ca^{2+} to activate the channel cooperatively. A preassembled gating ring is therefore a prerequisite for MthK gating.

RESULTS

Structure Determination of the Ligand-free MthK Gating Ring

The MthK RCK domain by itself can form a stable octameric gating ring at physiological pH with or without Ca^{2+}. Initial crystallization of the wild-type RCK domain in the absence of Ca^{2+} produced only poorly diffracting crystals. Well-diffracting crystals were obtained from the RCK domain of a mutant channel, D184N, in which one of the Ca^{2+}-binding residues, Asp184, was replaced by Asn (Jiang et al., 2002a). The D184N mutant exhibits the same single-channel conductance as the wild-type channel but has a much lower open probability and a decreased Ca^{2+} sensitivity (Figure 1B). It is possible that the mutation provides extra stability to the closed form of the gating ring and leads to better-diffracting crystals.

The crystal was of space group $C222_1$ with unit-cell dimensions of a = 174.1 Å, b = 181.0 Å, c = 252.7 Å, $\alpha = \beta = \gamma = 90^\circ$ and contained eight RCK subunits in one asymmetric unit. The structure was determined using molecular replacement and was refined to 2.8 Å with R_{work} of 21.2% and R_{free} of 25.4% (see Experimental Procedures and Table S1 in the Supplemental Data available with this article online). Interestingly, rather than forming a single octameric gating ring, the eight RCK subunits in the asymmetric unit are involved in the assembly of two gating rings, each of which consists of four of the subunits in the asymmetric unit along with their crystallographic 2-fold-related counterparts (Figure 1C). Surprisingly, these two gating rings are not in the same conformation: One is in the closed state, and the other is in a partially open state.

Overall Structure of the MthK Gating Ring in the Closed State

The closed gating ring maintains the same 422 molecular symmetry as the open gating ring from the MthK structure (Figures 1D and 1E). In the context of the entire channel, the eight gating-ring-forming RCK subunits can be divided into two groups: the top four (subunits A1 to A4, in yellow and brown), which are connected to the pore through four peptide linkers, and the bottom four (subunits B1 to B4, in gray), which are soluble RCK domains coexpressed with the channel and coassembled in the cytosol (Figures 1A and 1D). These two groups of RCK domains form a complementary interlock—each subunit only makes extensive contacts with two neighboring subunits from the other group through two distinct interfaces, the flexible and

(D) Stereoview of the closed MthK gating ring in ribbon representation. Subunits A1 to A4 are in yellow and brown; subunits B1 to B4 are in gray. Flexible and assembly interfaces alternate around the ring and hold the eight RCK subunits in an enclosed ring. Open square represents the 4-fold molecular symmetry.

(E) CPK models of the gating ring in the closed (left) and open (right) state. Subunits are colored as in (D). The molecular symmetries are represented by the square (4-fold) and arrows (2-fold). "New interface" indicates the new interfacial contacts between two neighboring subunits within the same group. Blue spheres are the Cα atoms of the N-terminal residues (Arg116) from the top four subunits. The open gating ring is from the MthK structure (PDB ID code 1LNQ).

(F) In the closed ring, two neighboring subunits (yellow and brown) within the same group form new interfacial contacts (upper panel) that are absent in the open gating ring (lower panel).

assembly interfaces. These interfaces alternate around the ring and hold the eight RCK subunits in an enclosed ring architecture. Protein contacts at the flexible interface are extremely extensive, with 3500 Å^2 of buried solvent-accessible surface area per subunit. The two RCK subunits dimerized through this interface can have various relative positions, indicating the flexible nature of this interface (Dong et al., 2005). The assembly interface is less extensive, with about 760 Å^2 of buried solvent-accessible surface area per subunit, and was previously suggested to be fixed (Jiang et al., 2002a). However, two RCK subunits interacting through this interface can also have different relative orientations, indicating that this interface is not truly fixed. We rename this interface the assembly interface in this study for its role in the assembly of the gating ring.

Compared to the open state, the gating ring in the closed state is taller but has a smaller diameter: It has a height of 52 Å and a 15 Å wide central hole, whereas the open ring is 47 Å tall and has a 20 Å wide central hole (Figure 1E). The most important difference is the diagonal distance between two Cα atoms of the N-terminal residues (Arg116, blue sphere), which are located at the outer rim of the gating ring and are linked to the pore in the functional channel. This distance changes from 66 Å in the closed state to 74 Å in the open state. This expansion of the gating ring from closed to open likely exerts a lateral force on the pore-lining inner helices that can lead to the opening of the channel.

In addition to changes in the overall shape, there is an increase in intersubunit contacts in the closed gating ring: The buried surface area increases from 4300 Å^2/subunit in the open state to 4590 Å^2/subunit in the closed state. Most of the increase can be attributed to the new interfacial contacts between two neighboring subunits within the same group (new interface in Figure 1E). These involve salt bridges and a hydrogen bond between E125, K150, and R154 from one subunit and R166, E146, and the main-chain carbonyl oxygen of H161 from the other, respectively (Figure 1F)

Interfacial Conformational Changes between the Gating Rings of Closed and Open States

The opening and closing of the gating ring result from the rigid-body movements of individual RCK subunits around two hinge points. The first is at the loop (around S230) between the N-terminal Rossmann-folded subdomain (the N-terminal lobe) and the helix-turn-helix (αF-turn-αG) intermediate subdomain. The other is at the loop (around T261) between the intermediate subdomain and the C-terminal subdomain (Figure 2A). The C-terminal subdomain participates in part of the dimerization interactions at the flexible interface with its counterpart and protrudes at the outer perimeter of the gating ring. This subdomain moves in conjunction with the N-terminal lobe, resulting in a rotation around the molecular 2-fold axis across the flexible interface. However, such movement has no direct effect on the gating-ring conformation. The N-terminal lobe, on the other hand, forms the core of the gating ring, and its movement changes the relative position between the two subunits across the flexible and assembly interfaces and results in a change in gating-ring shape.

Through extensive protein-protein contacts at the flexible interface, two RCK subunits form a bilobed dimer with a deep cleft in between (Figure 2A) (Dong et al., 2005; Jiang et al., 2002a). This form of dimer, which will be referred to as a flexible dimer, is always observed under nondenaturing conditions and can be considered the basic building block of the gating ring. The two N-terminal lobes within the flexible dimer can move relative to each other, resulting in a shape change at the cleft. As shown in the superimposition in Figure 2B, the flexible dimer in the closed gating ring has a narrower V-shaped cleft than that in the open gating ring, with an angle of 70° compared to 88°. The schematic drawings in Figure 2B illustrate the conformational change of a flexible dimer from closed to open state: Each lobe undergoes a 9° rotation away from its partner around the hinge point at the base of the cleft and an 8° twist around the dipole axis of helix αF. Since this movement is within a flexible dimer, it will be considered an intradimer conformational change.

The assembly interface, so named because of its role in assembling four flexible dimers into an octameric gating ring, is located at the external faces of helices αD and αE in the N-terminal lobe (Figure 2A). Compared to the flexible interface, protein contacts at this interface are less extensive and involve hydrophobic interactions at the center surrounded by salt bridges and hydrogen bonds. Two subunits interacting through the assembly interface undergo an approximately 18° rotation relative to each other between closed and open states (Figure 3A). This movement will be considered an interdimer conformational change since it is between two flexible dimers. The conformational change at the assembly interface maintains the protein contacts at the core of the interface, which consist of hydrophobic contacts from the I192 and L196 residues and hydrogen bonds between the two nitrogen atoms (δ1 and ε2) of His193 and the side chains of S189 and N216 (Figures 3B and 3C). However, there is a rearrangement of protein-protein interactions in the surrounding area: The salt bridge between R166 and E215 observed in the open state is disrupted and replaced by a new salt bridge between D163 and R213, along with a new hydrogen bond between E215 and the backbone of V167 in the closed state, and M222, which forms the edge of the hydrophobic patch in the open state, swings away from the core of the interface and no longer participates in hydrophobic interactions in the closed state (Figures 3B and 3C). Despite this rearrangement, the extent of protein contacts at this interface remains similar in both states.

Ligand-Binding Site

The Ca^{2+}-bound, open MthK structure reveals that two Ca^{2+} ions bind at the base of the cleft within each flexible dimer, very close to the hinge point (residue S230) of the intradimer movement (Jiang et al., 2002a) (Figure 2A).

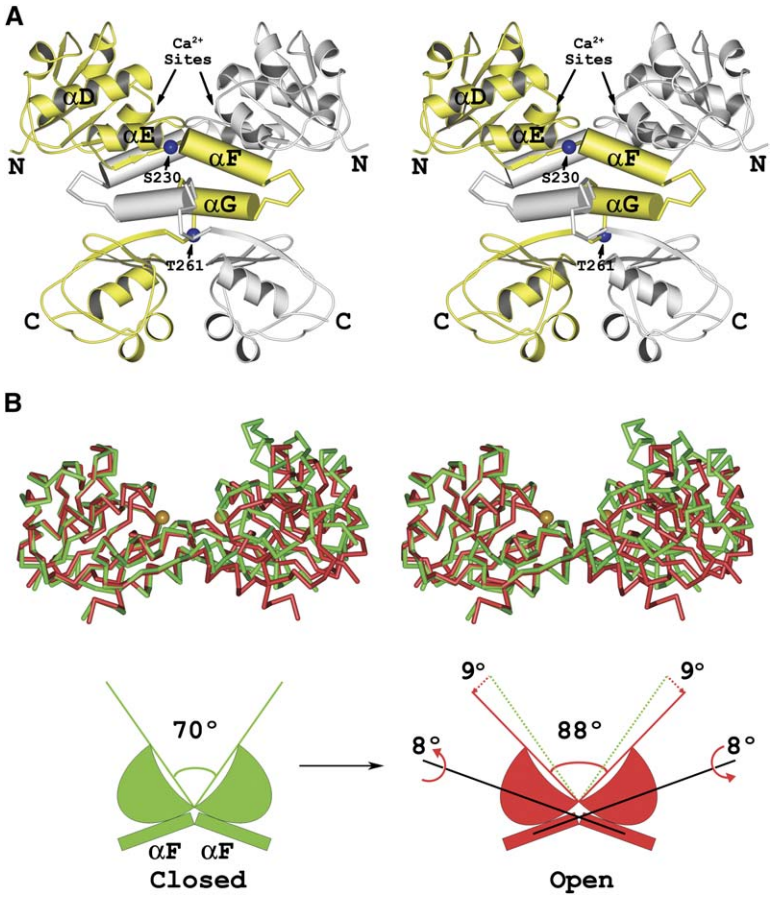

Figure 2. Intradimer Conformational Changes at the Flexible Interface

(A) Stereoview of a flexible dimer from the closed gating ring. Two subunits are colored yellow and gray. Arrows indicate the locations of Ca^{2+}-binding sites. Two blue spheres represent the Cα atoms of S230 and T261. Residues from the N terminus to S230 form the N-terminal subdomain (N-terminal lobe), residues from S230 to T261 form a helix-turn-helix (αF-turn-αG) intermediate subdomain, and residues from T261 to the C terminus form the C-terminal subdomain. The assembly interface locates at the external face of helices αD and αE. All labels are marked on the yellow subunit.

(B) Superimposition of flexible dimers from closed (green) and open (red) gating rings, with their C-terminal subdomains and αG helices removed for clarity. Gold spheres represent the bound Ca^{2+} ions in the open conformation. The schematic drawing illustrates the intradimer conformational changes between the closed and open states.

This Ca^{2+} site is located ideally to mediate conformational changes across the flexible interface upon Ca^{2+} binding. The chelation of each Ca^{2+} involves three acidic residues (Asp184, Glu210, and Glu212) and three water molecules (Dong et al., 2005). While Asp184 contributes both carboxylate oxygen atoms in the chelation of the Ca^{2+}, Glu210 and Glu212 only contribute one of their carboxylate oxygen atoms.

A structural comparison of the gating rings between closed (Ca^{2+}-free) and open (Ca^{2+}-bound) states reveals subtle differences in the vicinity of the Ca^{2+}-binding sites (Figure 4A). This is expected, given the close proximity of the Ca^{2+}-binding sites and the hinge point; small conformational changes induced by Ca^{2+} binding are amplified distally, such as at the N terminus of the RCK domain. Two noticeable differences are observed around the Ca^{2+} sites (Figures 4B and 4C). First, the side chain of Glu212 chelating the Ca^{2+} in the open state swings away from the binding site in the closed state. Second, in the open state, the two phenylalanine (Phe232) residues separating the two Ca^{2+} sites align almost in plane, with a distance of 3.1 Å between them, as if they were compressed from both sides; in the closed state, they become offset and lose the planar alignment, with a distance of 4.1 Å between them. Although the closed gating-ring structure is obtained from the D184N mutant, the flexible dimer of this closed gating ring has virtually the same structure at the Ca^{2+}-binding sites as a previously determined unliganded RCK dimer structure (PDB ID code 2AEM) (Dong et al., 2005), suggesting that the mutation does not induce structural changes at the Ca^{2+}-binding sites.

How does Ca^{2+} binding change the shape of the cleft, leading to an expansion of the gating ring? Electrostatic interactions provide one possibility. Across the flexible interface, the two bound Ca^{2+} ions in the open gating ring are in close proximity (~10 Å apart), separated solely by two phenylalanine residues (Figure 4C). The combination of close proximity and a nonpolar environment between ions at the flexible interface suggests that Ca^{2+} ions at these binding sites may have strong, repulsive electrostatic interactions. Another possibility could relate to stereo packing. In the Ca^{2+}-bound state, the partially charged carboxylate oxygen from Glu212 is positioned in close proximity (~3.7 Å) to the aromatic ring of Phe232, which may interfere sterically with closure of the cleft. These two possibilities are not mutually exclusive. In both cases, Ca^{2+} causes a repulsion between the two lobes of the flexible dimer, leading to a widening of the cleft and stabilization of the open conformation. Two phenylalanine residues reside at the very bottom of the cleft, with their aromatic side chains

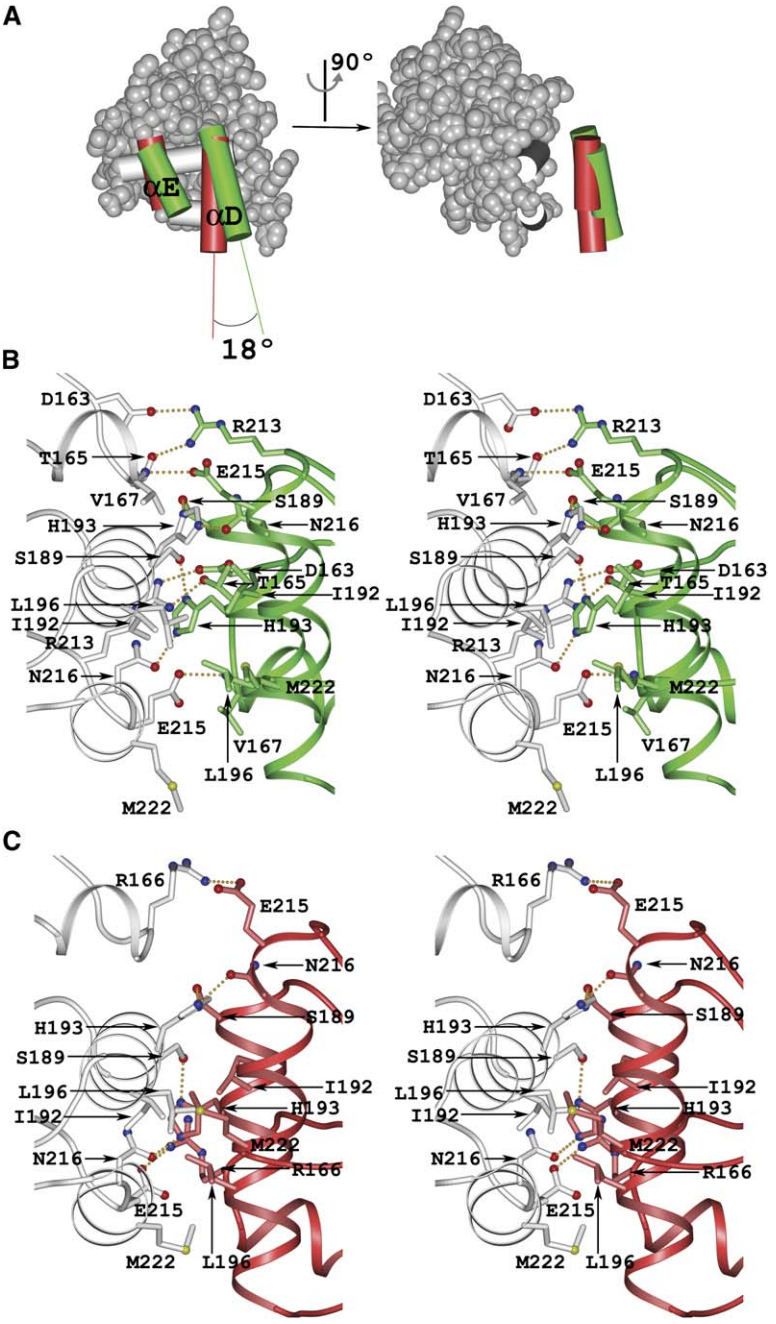

Figure 3. Interdimer Conformational Changes at the Assembly Interface

(A) Relative rotation between two subunits at the assembly interface (external face of αD and αE) when the gating ring moves between closed and open states. One subunit is in gray CPK representation, with its αD and αE drawn as cylinders. Only αD and αE are shown in the other subunit, as green cylinders in the closed state and red cylinders in the open state.

(B) Stereoview of the interdimer interactions at the assembly interface in the closed gating ring.

(C) Stereoview of the interdimer interactions at the assembly interface in the open gating ring.

forming a wall that partitions the two Ca^{2+} sites, and seem to be well positioned to mediate the effect of Ca^{2+} binding on channel gating. Indeed, a F232A mutation gives rise to a channel that exhibits the same conductance as the wild-type channel but has a much lower open probability and decreased Ca^{2+} sensitivity (Figure 4D).

Structure of a Partially Open Gating Ring

In addition to the closed gating ring, a partially open gating-ring structure was also observed in the same crystal (Figure 1C and Figure 5A). The four flexible dimers forming this partially open gating ring are in two different conformations: Three of them adopt a closed conformation similar to the ones in the closed gating ring, with a root-mean-square deviation (rmsd) of 0.76 Å in Cα positions, while the fourth is wide open. Consequently, the molecular symmetry of the gating ring is reduced to 2-fold. In the crystal, this molecular dyad coincides with a crystallographic 2-fold axis (Figure 1C). This asymmetrical gating ring has different diagonal distances between Cα atoms of the N-terminal residues (Arg116, blue sphere), with a longer distance of 74 Å similar to that of an open gating ring and a shorter

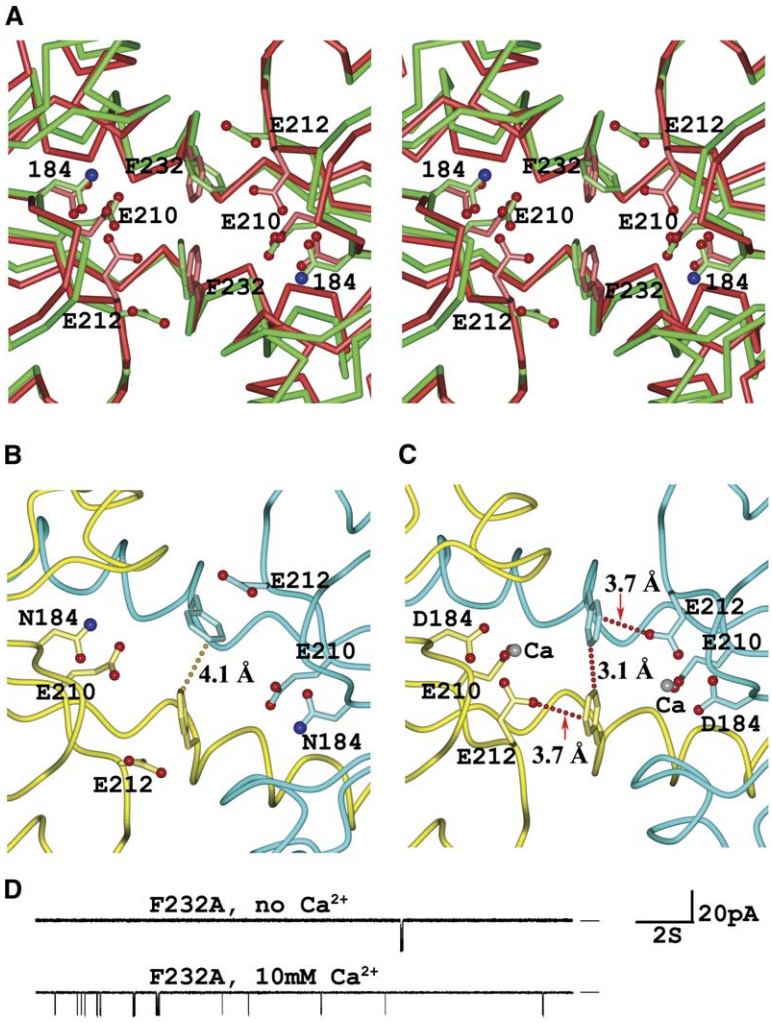

Figure 4. Conformational Changes around the Ca^{2+}-Binding Sites

(A) Stereoview of the structures around the two Ca^{2+}-binding sites at the base of the cleft in the gating rings of the closed (green) and open (red) states. Residue 184 is Asp in the open gating ring (wild-type) and Asn in the closed gating ring (D184N mutant).

(B) Structure around Ca^{2+}-binding sites in the closed gating ring. Two subunits are colored yellow and cyan.

(C) Structure around Ca^{2+}-binding sites in the open gating ring (PDB ID code 1LNQ). Silver spheres represent the two bound Ca^{2+} ions.

(D) Single-channel traces of F232A mutant in the absence and presence of 10 mM $CaCl_2$. Currents were recorded at −100 mV with an intracellular pH of 8.0 and 150 mM symmetrical KCl. Lines to the right mark the zero current level.

one of 66 Å corresponding to that of a closed gating ring (Figure 5A and Figure S1).

From the closed to the partially open state, one flexible dimer in the gating ring undergoes conformational changes while the others remain closed (Figure 5B). This conformational change involves a 16° rotation away from its partner and a 15° twist around the dipole axis of helix αF by each N-terminal lobe (Figure 5C). This movement is almost twice as extensive as the intradimer conformational change between the gating rings of the closed and open states (Figure 2B). This more extensive movement has two consequences. At the flexible interface, it gives rise to a wider opening at the cleft between the two lobes with an angle of 102°; at the assembly interface, each lobe has an 18° rotation relative to the neighboring subunit, allowing the wide-open flexible dimer to engage in open-state interdimer interactions with its neighboring closed dimers. Therefore, even with a wide-open conformation within one of its dimers, the partially open gating ring maintains an enclosed but asymmetrical ring architecture by having a mixture of open- and closed-state interdimer contacts at the assembly interfaces (Figure 5A).

It is interesting to note that the conformation of the wide-open flexible dimer in the partially open gating ring has also been observed in the structures of isolated RCK dimers with and without bound Ca^{2+} (Dong et al., 2005), confirming that the flexible interface is indeed flexible and that the two RCK subunits can adopt multiple conformations across this interface. However, in the context of a gating ring, the stabilities of these multiple conformations are influenced by the interdimer interactions at the assembly interfaces.

MthK Gating Requires the Preassembly of the Gating Ring

The stability of the MthK gating ring is pH dependent. Lower pH disrupts the octameric gating ring into dimers by destabilizing the interdimer interactions across the assembly interfaces (Dong et al., 2005). As shown in Figure 6A, purified RCK domains remain octameric at pH 7.5, become predominantly dimeric at pH 6.5, and

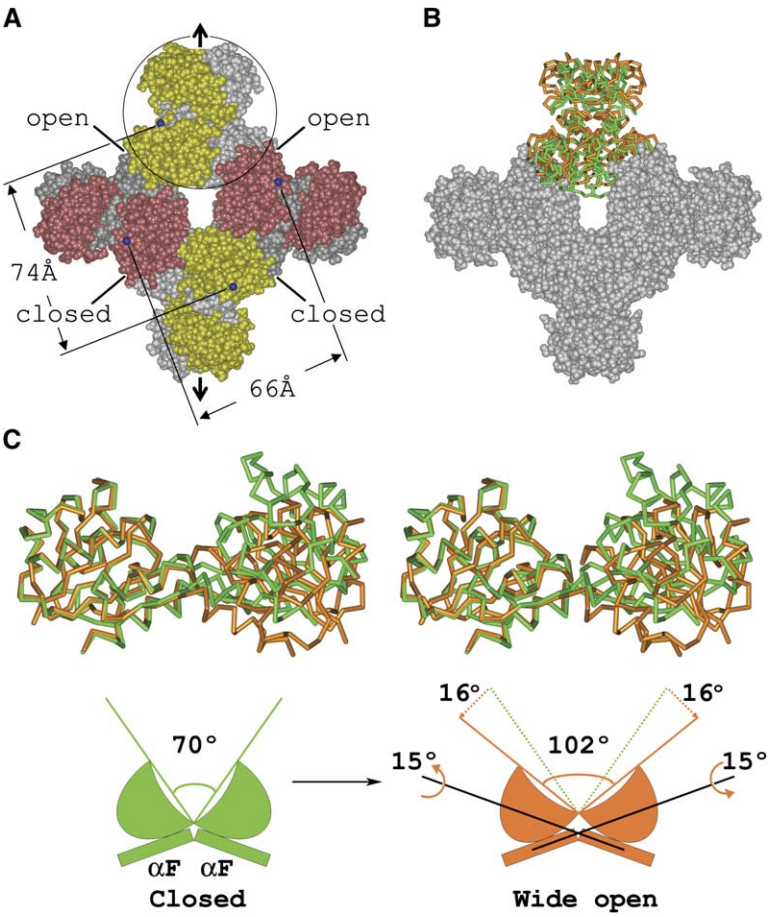

Figure 5. Structure of a Partially Open Gating Ring

(A) CPK model of the gating ring in a partially open state. One flexible dimer (circled) adopts a wide-open conformation. The interdimer conformations at the assembly interfaces are a mixture of open and closed states as indicated. Arrow indicates the 2-fold molecular symmetry, which coincides with a crystallographic 2-fold rotation axis. Blue spheres are Cα atoms of the N-terminal residues (Arg116). (B) For a gating ring to move from a closed to partially open state, only one flexible dimer undergoes a conformation change. The Cα traces represent this moving flexible dimer in the closed (green) and partially open (orange) gating rings. The three flexible dimers that remain closed are shown in CPK representation (gray). (C) Superimposition of flexible dimers in closed (green) and wide open (orange) states, with their subdomains and αG helices removed for clarity. The schematic drawing illustrates the intradimer conformational changes between the closed and wide-open flexible dimers.

exist in a mixture of oligomeric states between dimers and octamers at pH 7.0.

To study the pH effect on MthK gating, we measured channel activity at different pHs in synthetic lipid bilayers. While changes in pH of the solution at the extracellular side have no obvious effect on channel activity, the pH changes at the intracellular side profoundly affect the channel open probability. In the presence of 10 mM Ca^{2+}, the channel rarely opens at a pH below 7.0, whereas its open probability increases dramatically at pHs above 7.0 (Figures 6B and 6C). Figure 6B also shows that the pH effect on channel open probability is reversible. This is in agreement with the observed pH sensitivity of gating-ring stability, indicating that the disruption of the gating ring at lower pH desensitizes Ca^{2+} activation of the channel. The presence of eight Ca^{2+}-binding sites and the allosteric gating-ring conformational changes suggest a cooperative Ca^{2+} activation of the channel. Such activation requires an intact gating-ring assembly. Indeed, at lower pH (<7.0), Ca^{2+} has little effect on channel activity, while at higher pH, the channel open probability shows a steeply sigmoidal relationship with [Ca^{2+}] (Figure 6D), consistent with the proposal that the assembly of the gating ring is a prerequisite for Ca^{2+} gating.

It is unclear what causes the pH sensitivity of MthK. The following observations lead us to postulate that His193 is responsible for the pH dependence of gating-ring stability: First, lower pH disrupts the octameric gating ring by destabilizing the assembly interface; second, the transition between octamers and dimers occurs at a pH around 7.0, near the pKa of histidine; and third, His193 resides at the core of the assembly interface. Numerous mutations at His193 (H193F, A, L, N, Q, and some double mutations) have been generated to test this hypothesis. However, because His193 is located at the center of the assembly interface, it is highly sensitive to mutagenesis, and all mutations tested destabilize the assembly interface. In the absence of a stable mutant channel, we are currently unable to validate our hypothesis directly.

The pH sensitivity of channel gating may be unique to MthK. In most other RCK domains, hydrophobic amino acids are conserved at positions equivalent to His193. It is likely that pH does not have the same effects on other RCK-regulated channels as it does on MthK. Whether this pH sensitivity of the MthK channel is physiologically relevant in *Methanobacterium thermoautotrophicum* requires further investigation. Nonetheless, it is clear that

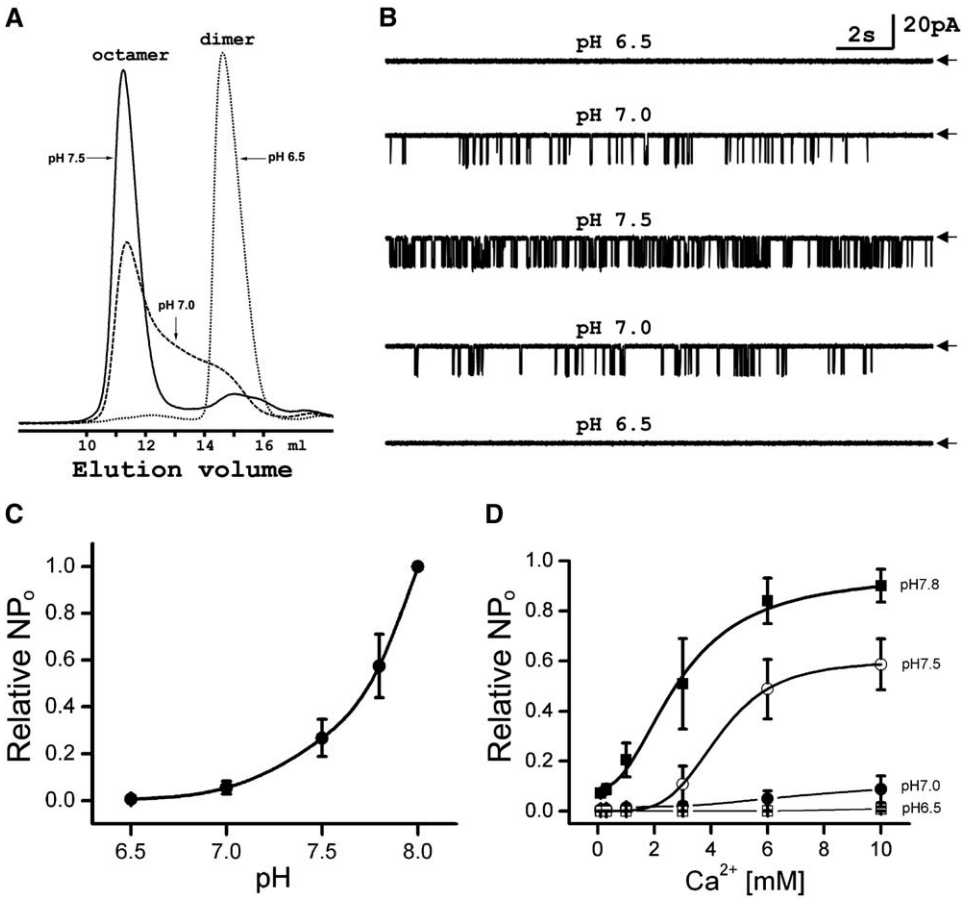

Figure 6. Ca^{2+} and pH Regulation of MthK Gating

(A) Profile of MthK RCK domains on a gel filtration column at pH 6.5, 7.0, and 7.5.

(B) Single-channel traces of MthK at various intracellular pHs with 10 mM Ca^{2+}. The pH of the solution is increased from 6.5 to 7.5 and then decreased back to 6.5. Arrows mark the zero current level.

(C) Relative open probability (Relative NP_o) of the MthK channel at various intracellular pHs with 10 mM Ca^{2+}. NP_o measurement at each pH was normalized against the measurement of the same bilayer at pH 8.0. Data are mean ± SEM of six measurements.

(D) Ca^{2+} activation of the MthK channel at various intracellular pHs. NP_o of each measurement was normalized against the measurement of the same bilayer after adjusting the pH to 8.0 and $[Ca^{2+}]$ to 10 mM at the intracellular side. The smooth lines are fits with the Hill equation, $P_o = P_{max}/(1 + (K_{1/2}/[Ca^{2+}])^n)$, where n is the Hill coefficient and $K_{1/2}$ is the $[Ca^{2+}]$ required for P_o to reach half of maximum. At pH 7.5, n = 4.3 and $K_{1/2}$ = 4.1 mM; at pH 7.8, n = 2.2 and $K_{1/2}$ = 2.9 mM. Data are mean ± SEM of 4–6 measurements.

pH modulates Ca^{2+} gating in the MthK channel by affecting gating-ring stability.

DISCUSSION

Mechanism of MthK Gating

The data presented here have allowed us to elucidate a possible mechanism of RCK-regulated gating of the MthK channel (Figure 7A). The opening and closing of MthK is controlled by both pH and Ca^{2+}. Ca^{2+} affects channel gating by influencing intradimer conformational changes at the flexible interface, while pH affects channel gating by mediating the stability of interdimer interactions at the assembly interface. Although the gating-ring architecture is no longer preserved at lower pH, the channel still has eight RCK domains (as four flexible dimers) attached to the intracellular side of the pore. This occurs due to the tetramerization of the pore domains and extensive protein-protein interactions at the flexible interfaces. Without forming a gating ring, Ca^{2+}-induced conformational changes at the flexible interfaces can no longer be coupled to a gating-ring movement, and the channel is therefore desensitized. At higher pH, close proximity allows the four flexible dimers to be readily assembled into a stable gating ring that exists in equilibrium between open and closed conformations. Ca^{2+} binding cooperatively shifts the equilibrium toward the open state. The expansion of the outer rim of the gating ring by about 8 Å from closed to open states results in an opening of the channel gate to about 12 Å, large enough to allow hydrated K^+ ions to pass freely.

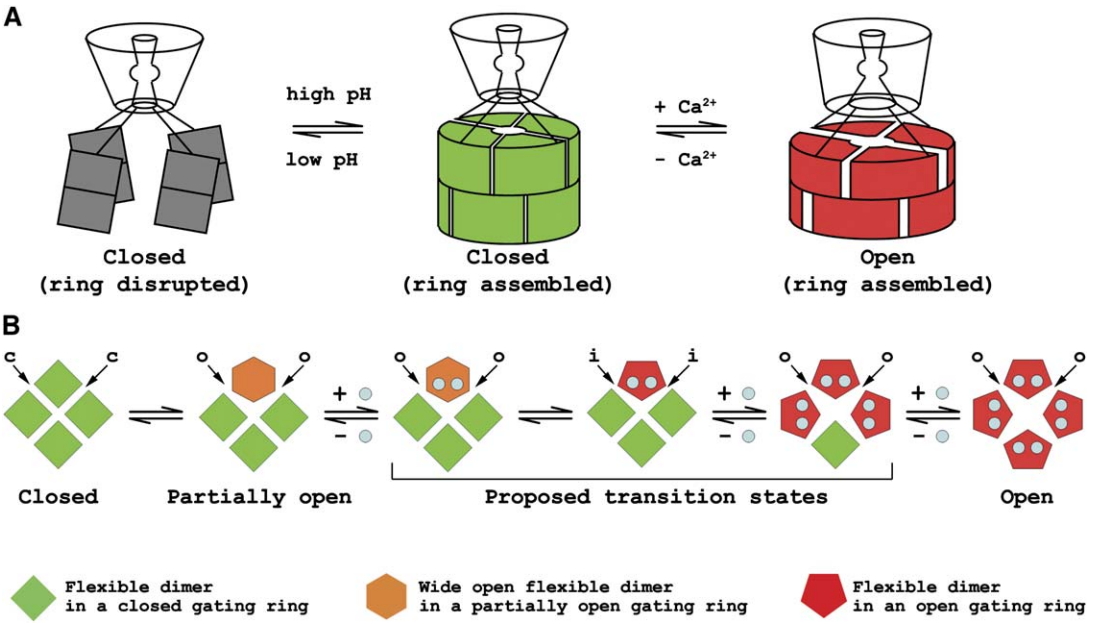

Figure 7. Proposed Mechanism of MthK Gating

(A) Proposed gating mechanism of MthK. Funnel represents the membrane-spanning ion-conduction pore. The gating rings in closed and open states are colored green and red, respectively, and are tethered to the pore through four peptide linkers. The four flexible dimers that are unable to form a gating ring at lower pH are represented as gray rectangles attached to the pore.

(B) Proposed gating-ring transition between closed and open states. Green squares, orange hexagons, and red pentagons represent the flexible dimers in the closed, partially open (wide-open conformation), and open states, respectively. Cyan spheres represent Ca^{2+} ions. The conformations of interdimer interactions between the moving flexible dimer and its neighbors are indicated as c for closed conformation, o for open conformation, and i for an intermediate state between open and closed conformations.

How are the conformational changes of the gating ring coupled to pore opening and closing in MthK? In our opinion, the most likely possibility is through the four covalent linkers between the gating ring and the pore. In the open MthK structure, the 17 residue linker, which accounts for a distance of 25 Å between the N terminus of the gating-ring-forming RCK domains and the C terminus of the pore-lining inner helix, was not defined due to poor electron density (Jiang et al., 2002a). In order to couple the conformational changes between the gating ring and the pore, the linkers are expected to have a substantially rigid structure. We suspect that the 17 linker residues unresolved in the MthK structure form a helix that gives rise to a length of 25 Å, consistent with the intervening distance between the pore and the gating ring. In agreement with the putative helical structure of the linker, mutagenesis studies of the eukaryotic large-conductance Ca^{2+}-gated K^+ channel (BK channel), which is regulated by RCK domains, have shown that modifications of the linker lengths have profound effects on channel activity and that the four linkers couple the gating ring to the pore by acting as a passive spring (Niu et al., 2004).

Allosteric Transition of the Gating Ring between Closed and Open States

The interfacial conformational changes of the gating ring at the two distinct interfaces exhibit quite different characteristics. Across the flexible interface, two subunits can adopt multiple conformations with little effect on the extent of the interfacial contacts. The conformational change at the assembly interface, on the other hand, is more restrictive since such movement results in a rearrangement of interfacial contacts. The fact that Ca^{2+} ions bind at the base of the cleft and directly influence the conformational change across the flexible interface suggests that the intradimer movements within each flexible dimer determine the gating-ring conformation. In response to the intradimer movements, the interdimer interactions at the assembly interfaces switch between open and closed states in order to maintain a stable gating ring.

The observation of a closed and a partially open gating ring in the same crystal suggests that the gating ring can adopt either conformation in the absence of ligand. We have also determined the crystal structure of the ligand-free MthK gating ring from a different crystal form, which has a $P2_1$ space group and contains five gating rings in an asymmetric unit. The structure shows all five gating rings in the closed conformation (Figure S2), suggesting that, in the absence of Ca^{2+}, the closed gating ring is more stable.

We believe the partially open gating ring represents an intermediate conformation between open and closed states. Its structure, along with those of the open and closed gating rings, leads us to postulate a transition

process of the gating ring from closed to open as illustrated in the schematic drawing (Figure 7B; see also Movie S1). Instead of considering the conformational change of individual subunits, the proposed model is simplified by treating each flexible dimer as one moveable unit. In the absence of Ca^{2+}, the gating ring switches between the closed and partially open states. This conformational change involves one flexible dimer moving between closed and wide-open states while the interdimer interactions at its assembly interfaces switch between closed and open states accordingly. The wide-open flexible dimer is apparently more accessible for Ca^{2+} binding. Upon Ca^{2+} binding, this dimer adopts the open conformation, which may result in unstable interdimer contacts (in a state between open and closed conformations) with its neighboring closed dimers. In response, the two neighboring dimers tend to move toward the open state, favoring Ca^{2+} binding, followed in turn by the opening of the fourth dimer. This leads to the formation of an open gating ring stabilized by open-state interdimer contacts.

The Octameric Gating Ring Is the Functional Assembly of RCK Domains

Our structural study clearly demonstrates that the gating of MthK requires the assembly of an octameric gating ring. To form this assembly, an extra copy of the soluble RCK domain is expressed from the *MthK* gene using an internal starting site (Met107) and is coassembled with the channel protein. This phenomenon of expressing both the full-length channel and a soluble ligand-binding domain from the same gene has also been observed in several other RCK-regulated prokaryotic K^+ channels (Hellmer and Zeilinger, 2003; Kuo et al., 2003; Ptak et al., 2005), suggesting a general theme utilized by this group of K^+ channels to generate an intracellular octameric gating ring whose conformational changes control the opening and closing of the ion-conduction pore. It is interesting to note that each BK channel subunit contains two tandem intracellular RCK domains at the C terminus. It is likely that the RCK domains in a functional BK tetramer form the same gating-ring architecture (Pico, 2003). Although the Ca^{2+}-binding site in the BK channel is different from that in MthK (Bao et al., 2002; Bian et al., 2001; Schreiber and Salkoff, 1997; Xia et al., 2002; Magleby, 2003), the Ca^{2+}-induced gating-ring conformational change in BK may be similar to that observed in MthK.

What is the functional assembly of RCK domains in K^+-transporter systems? Based on the structural studies of two KTN domains from KtrA, the soluble component of the bacterial Ktr K^+-uptake system, it was suggested that the functional assembly of KtrA is a dimer of dimers (Roosild et al., 2002, 2004). However, the structure and sequence conservation between KtrA and MthK RCK, especially of the two distinct dimerization interfaces, leads us to believe that KtrA and other RCK domains from K^+ transporters should also function as octameric gating rings. Indeed, recent structural studies and biochemical characterization of KtrA clearly demonstrate that it forms an octameric gating ring both in solution and in crystals in various ligand-bound states (Albright et al., 2006), providing compelling evidence to support the suggestion that RCK domains function as an octamer in both K^+ channels and transporters.

Despite the diversity of ligands for RCK domains, the structures of RCK domains from K^+ channels and transporters reveal a common location for ligand binding: at the cleft within the flexible dimer. It is likely that ligand binding induces a similar kind of intradimer conformational change at the flexible interface that can be propagated through the protein-protein contacts at the assembly interfaces, resulting in a shape change of the gating ring.

EXPERIMENTAL PROCEDURES

Protein Expression and Purification

The *MthK* gene, which also expresses the soluble RCK domain, was cloned into a pQE70 vector (QIAGEN) with a thrombin cleavage site between the channel and the C-terminal hexahistidine tag. The channel was overexpressed in *E. coli* SG13009 cultures by induction with 0.4 mM isopropyl-β-D-thiogalactopyranoside (IPTG) at $A_{600} \sim 0.8$. Cells were harvested and lysed in 50 mM Tris-HCl (pH 8.0) and 250 mM NaCl containing leupeptin, pepstatin, aprotinin, and PMSF (Sigma) to inhibit proteases. The supernatant of the cell lysate, containing an excess of the soluble RCK domain, was collected after centrifugation at 21,000 × g for 20 min. The RCK domain was purified on a Talon Co^{2+} affinity column (Clontech) and eluted with 20 mM Tris-HCl (pH 8.0), 250 mM NaCl, and 300 mM imidazole. Protein eluted from the Co^{2+} column was incubated for 3 hr at ~20°C in the presence of 1.0 unit of thrombin (Roche) per 2.0 mg of protein to remove the hexahistidine tag and further purified on a Superdex 200 (10/30) gel filtration column (Pharmacia) in 20 mM Tris-HCl (pH 8.0) and 250 mM NaCl. The mutant version (D184N or F232A) of the *MthK* gene was generated using QuikChange site-directed mutagenesis. The preparation of the D184N RCK domain was the same as described above. For functional analysis, MthK and its mutants were purified in n-decyl-β-D-maltoside detergent (DM from Anatrace) using the same method as described (Jiang et al., 2002a).

Gel filtration chromatography (Superdex 200, 10/30 column) was used to determine the oligomeric states of the wild-type RCK domains at different pHs. Purified RCK octamers (as described above) were dialyzed against solutions of 250 mM NaCl and 20 mM buffer with various pHs (Tris-HCl [pH 7.5], HEPES [pH 7.0], and MES [pH 6.5]) and then loaded onto the gel filtration column equilibrated with the same solutions.

Crystallization and Structure Determination

The purified D184N RCK was concentrated to ~6 mg/ml for crystallization. Crystals were grown by sitting-drop vapor diffusion at 20°C by mixing equal volumes of protein and reservoir solution of 0.6 M Na/K PO_4 (pH 8.0).

All data were collected at the Argonne National Laboratory Structural Biology Center 19ID beamline at the Advanced Photon Source at −180°C under a nitrogen stream. The data sets were processed and scaled with HKL2000 (Otwinowski and Minor, 1997). The structure was solved by molecular replacement using the program Phaser (McCoy et al., 2005; Storoni et al., 2004). Initial search using the RCK N-terminal region (residues 116–247) from the open MthK structure (PDB ID code 1LNQ) located five subunits in the asymmetric unit, from which a dimer model containing two RCK N-terminal regions was generated. Subsequent searches using the dimer model successfully located all four partial dimers in the asymmetric unit. Although the

exact position of the C-terminal subdomain of each subunit could not be determined by molecular replacement, its approximate location could be defined by superimposing an RCK subunit from the MthK structure with each of the partial RCK models from the search result, allowing us to generate the molecular mask for phase improvement via solvent flattening and 8-fold NCS averaging using the program DM (CCP4, 1994). The electron density map calculated from the improved phases revealed the correct position of the RCK C-terminal subdomain. It also revealed that one RCK subunit, which forms a wide-open dimer with its crystallographic-symmetry-related counterpart, adopts a different conformation from the others. The 8-fold NCS was therefore released in the subsequent refinements. A complete model was constructed after iterative cycles of model building with XtalView (McRee, 1999) using the figure-of-merit-weighted $2|F_o| - |F_c|$ maps calculated with ARPwARP-improved phases (Perrakis et al., 2001) and refinement with REFMAC (CCP4, 1994). The final model was refined to R_{work} and R_{free} of 21.2% and 25.4%, respectively, and contained eight RCK subunits with residues 116 to 336 for each subunit and 52 water molecules. The numbering in the model is based on the sequence of the MthK channel. 89.0% of the residues are in the most favored regions, 10.1% in additionally allowed regions, and 0.9% in generously allowed regions on a Ramachandran plot.

Protein Reconstitution and Functional Analysis

The MthK channel and its mutants were reconstituted into lipid vesicles composed of 1-palmitoyl-2-oleoyl-phosphatidylethanolamine (POPE, 7.5 mg/ml) and 1-palmitoyl-2-oleoyl-phosphatidylglycerol (POPG, 2.5 mg/ml) at a protein-to-lipid ratio of 2–5 μg/mg using the same method as described (Heginbotham et al., 1999) except for the following modifications: DM detergent was used to solubilize the lipid, and dialysis (against a buffer of 10 mM HEPES [pH 7.2], 450 mM KCl, and 4 mM NMG) was used to slowly remove the detergent from the detergent/lipid/protein mixture.

Channel activity was studied in a vertical lipid-bilayer membrane in which a planar lipid bilayer of POPE (15 mg/ml) and POPG (5 mg/ml) in decane was painted over a hole (~200 μm) in a polystyrene partition separating the internal and external solutions. To induce fusion of channel-containing vesicles, the solution on the side where vesicles were added (external side) contained 150 mM KCl, 10 mM HEPES (pH 7.2) while the opposite side (internal side) contained 15 mM KCl, 10 mM HEPES (pH 7.2). After the appearance of channels in the membrane as monitored under voltage pulses, the KCl concentration on the internal side was increased to 150 mM. For pH adjustment, KOH or HCl (1 M stock) was added directly to the intracellular side and the pH was monitored by a pH meter. The pH on the extracellular side was kept at 7.2 in most experiments. Membrane voltage was controlled and current was recorded using an Axopatch 200B amplifier with a Digidata 1322A analog-to-digital converter (Axon Instruments). Currents were sampled at 10 kHz and low-pass filtered at 2 kHz. The software TAC (Bruxton Corporation) was used in statistical analysis of single-channel data.

Supplemental Data

Supplemental Data include two figures, one table, and one movie and can be found with this article online at http://www.cell.com/cgi/content/full/126/6/1161/DC1/.

ACKNOWLEDGMENTS

We thank A. Alam and P. Thibodeau for manuscript preparation; Drs. J. Cabral, R. MacKinnon, and E. Goldsmith for discussion and critical review of the manuscript. Use of the Argonne National Laboratory Structural Biology Center beamlines at the Advanced Photon Source was supported by the US Department of Energy, Office of Energy Research. We thank the beamline staff for assistance in data collection. This work was supported by grants from the National Institutes of Health (GM071621), the Searle Scholars Program (04-A-101), and the Robert A. Welch Foundation (I-1578) to Y.J.

Received: February 16, 2006
Revised: May 8, 2006
Accepted: August 11, 2006
Published: September 21, 2006

REFERENCES

Albright, R.A., Ibar, J.-L.V., Kim, C.U., Gruner, S.M., and Morais-Cabral, J.H. (2006). The RCK domain of the KtrAB K^+ transporter: multiple conformations of an octameric ring. Cell *126*, this issue, 1147–1159.

Bakker, E.P., Booth, I.R., Dinnbier, U., Epstein, W., and Gajewska, A. (1987). Evidence for multiple K^+ export systems in Escherichia coli. J. Bacteriol. *169*, 3743–3749.

Bao, L., Rapin, A.M., Holmstrand, E.C., and Cox, D.H. (2002). Elimination of the BK(Ca) channel's high-affinity Ca(2+) sensitivity. J. Gen. Physiol. *120*, 173–189.

Bateman, A., Birney, E., Durbin, R., Eddy, S.R., Howe, K.L., and Sonnhammer, E.L. (2000). The Pfam protein families database. Nucleic Acids Res. *28*, 263–266.

Bellamacina, C.R. (1996). The nicotinamide dinucleotide binding motif: a comparison of nucleotide binding proteins. FASEB J. *10*, 1257–1269.

Bian, S., Favre, I., and Moczydlowski, E. (2001). Ca^{2+}-binding activity of a COOH-terminal fragment of the Drosophila BK channel involved in Ca^{2+}-dependent activation. Proc. Natl. Acad. Sci. USA *98*, 4776–4781.

CCP4 (Collaborative Computational Project, Number 4) (1994). The CCP4 suite: programs for protein crystallography. Acta Crystallogr. D Biol. Crystallogr. *50*, 760–763.

del Camino, D., and Yellen, G. (2001). Tight steric closure at the intracellular activation gate of a voltage-gated K(+) channel. Neuron *32*, 649–656.

del Camino, D., Holmgren, M., Liu, Y., and Yellen, G. (2000). Blocker protection in the pore of a voltage-gated K^+ channel and its structural implications. Nature *403*, 321–325.

Ding, S., Ingleby, L., Ahern, C.A., and Horn, R. (2005). Investigating the putative glycine hinge in Shaker potassium channel. J. Gen. Physiol. *126*, 213–226.

Dong, J., Shi, N., Berke, I., Chen, L., and Jiang, Y. (2005). Structures of the MthK RCK domain and the effect of Ca^{2+} on gating ring stability. J. Biol. Chem. *280*, 41716–41724.

Doyle, D.A., Morais Cabral, J., Pfuetzner, R.A., Kuo, A., Gulbis, J.M., Cohen, S.L., Chait, B.T., and MacKinnon, R. (1998). The structure of the potassium channel: molecular basis of K^+ conduction and selectivity. Science *280*, 69–77.

Heginbotham, L., LeMasurier, M., Kolmakova-Partensky, L., and Miller, C. (1999). Single streptomyces lividans K(+) channels: functional asymmetries and sidedness of proton activation. J. Gen. Physiol. *114*, 551–560.

Hellmer, J., and Zeilinger, C. (2003). MjK1, a K^+ channel from M. jannaschii, mediates K^+ uptake and K^+ sensitivity in E. coli. FEBS Lett. *547*, 165–169.

Jiang, Y., Pico, A., Cadene, M., Chait, B.T., and MacKinnon, R. (2001). Structure of the RCK domain from the E. coli K^+ channel and demonstration of its presence in the human BK channel. Neuron *29*, 593–601.

Jiang, Y., Lee, A., Chen, J., Cadene, M., Chait, B.T., and MacKinnon, R. (2002a). Crystal structure and mechanism of a calcium-gated potassium channel. Nature *417*, 515–522.

Jiang, Y., Lee, A., Chen, J., Cadene, M., Chait, B.T., and MacKinnon, R. (2002b). The open pore conformation of potassium channels. Nature *417*, 523–526.

Jin, T., Peng, L., Mirshahi, T., Rohacs, T., Chan, K.W., Sanchez, R., and Logothetis, D.E. (2002). The (beta)gamma subunits of G proteins gate a K(+) channel by pivoted bending of a transmembrane segment. Mol. Cell *10*, 469–481.

Kuo, M.M., Saimi, Y., and Kung, C. (2003). Gain-of-function mutations indicate that Escherichia coli Kch forms a functional K^+ conduit in vivo. EMBO J. *22*, 4049–4058.

Kuo, M.M., Haynes, W.J., Loukin, S.H., Kung, C., and Saimi, Y. (2005). Prokaryotic K(+) channels: from crystal structures to diversity. FEMS Microbiol. Rev. *29*, 961–985.

Liu, Y., Holmgren, M., Jurman, M.E., and Yellen, G. (1997). Gated access to the pore of a voltage-dependent K^+ channel. Neuron *19*, 175–184.

Liu, Y.S., Sompornpisut, P., and Perozo, E. (2001). Structure of the KcsA channel intracellular gate in the open state. Nat. Struct. Biol. *8*, 883–887.

Magidovich, E., and Yifrach, O. (2004). Conserved gating hinge in ligand- and voltage-dependent K^+ channels. Biochemistry *43*, 13242–13247.

Magleby, K.L. (2003). Gating mechanism of BK (Slo1) channels: so near, yet so far. J. Gen. Physiol. *121*, 81–96.

McCoy, A.J., Grosse-Kunstleve, R.W., Storoni, L.C., and Read, R.J. (2005). Likelihood-enhanced fast translation functions. Acta Crystallogr. D Biol. Crystallogr. *61*, 458–464.

McRee, D.E. (1999). XtalView/Xfit–A versatile program for manipulating atomic coordinates and electron density. J. Struct. Biol. *125*, 156–165.

Munro, A.W., Ritchie, G.Y., Lamb, A.J., Douglas, R.M., and Booth, I.R. (1991). The cloning and DNA sequence of the gene for the glutathione-regulated potassium-efflux system KefC of Escherichia coli. Mol. Microbiol. *5*, 607–616.

Nakamura, T., Yuda, R., Unemoto, T., and Bakker, E.P. (1998). KtrAB, a new type of bacterial K(+)-uptake system from Vibrio alginolyticus. J. Bacteriol. *180*, 3491–3494.

Niu, X., Qian, X., and Magleby, K.L. (2004). Linker-gating ring complex as passive spring and Ca(2+)-dependent machine for a voltage- and Ca(2+)-activated potassium channel. Neuron *42*, 745–756.

Otwinowski, Z., and Minor, W. (1997). Processing of X-ray diffraction data collected in oscillation mode. Methods Enzymol. *276*, 307–326.

Perozo, E., Cortes, D.M., and Cuello, L.G. (1999). Structural rearrangements underlying K^+-channel activation gating. Science *285*, 73–78.

Perrakis, A., Harkiolaki, M., Wilson, K.S., and Lamzin, V.S. (2001). ARP/wARP and molecular replacement. Acta Crystallogr. D Biol. Crystallogr. *57*, 1445–1450.

Pico, A. (2003). RCK domain model of calcium activation in BK channels. PhD thesis, Rockefeller University, New York.

Ptak, C.P., Cuello, L.G., and Perozo, E. (2005). Electrostatic interaction of a K^+ channel RCK domain with charged membrane surfaces. Biochemistry *44*, 62–71.

Roosild, T.P., Miller, S., Booth, I.R., and Choe, S. (2002). A mechanism of regulating transmembrane potassium flux through a ligand-mediated conformational switch. Cell *109*, 781–791.

Roosild, T.P., Le, K.T., and Choe, S. (2004). Cytoplasmic gatekeepers of K^+-channel flux: a structural perspective. Trends Biochem. Sci. *29*, 39–45.

Rossmann, M.G., Moras, D., and Olsen, K.W. (1974). Chemical and biological evolution of nucleotide-binding protein. Nature *250*, 194–199.

Schlosser, A., Hamann, A., Bossemeyer, D., Schneider, E., and Bakker, E.P. (1993). NAD^+ binding to the Escherichia coli K(+)-uptake protein TrkA and sequence similarity between TrkA and domains of a family of dehydrogenases suggest a role for NAD^+ in bacterial transport. Mol. Microbiol. *9*, 533–543.

Schreiber, M., and Salkoff, L. (1997). A novel calcium-sensing domain in the BK channel. Biophys. J. *73*, 1355–1363.

Storoni, L.C., McCoy, A.J., and Read, R.J. (2004). Likelihood-enhanced fast rotation functions. Acta Crystallogr. D Biol. Crystallogr. *60*, 432–438.

Xia, X.M., Zeng, X., and Lingle, C.J. (2002). Multiple regulatory sites in large-conductance calcium-activated potassium channels. Nature *418*, 880–884.

Zhao, Y., Yarov-Yarovoy, V., Scheuer, T., and Catterall, W.A. (2004). A gating hinge in Na^+ channels; a molecular switch for electrical signaling. Neuron *41*, 859–865.

Zhou, Y., Morais-Cabral, J.H., Kaufman, A., and MacKinnon, R. (2001). Chemistry of ion coordination and hydration revealed by a K^+ channel-Fab complex at 2.0 Å resolution. Nature *414*, 43–48.

Accession Numbers

The atomic coordinates and structural factors described herein have been deposited in the Protein Data Bank with the ID code 2FY8.